Ceramics International 43 (2017) 12546–12550

Contents lists available at ScienceDirect

Ceramics International

journal homepage: www.elsevier.com/locate/ceramint

The analysis of torsional shear strength test of sealants for solid oxide fuel cells

M. Fakouri Hasanabadi[a,b,*], M.A. Faghihi-Sani[a], A.H. Kokabi[a,*], J. Malzbender[b]

[a] Department of Materials Science and Engineering, Sharif University of Technology, Azadi Avenue, P. O. Box 11155-9466, Tehran, Iran
[b] Forschungszentrum Jülich GmbH, Institute for Energy and Climate Research, IEK-2, 52425 Jülich, Germany

ARTICLE INFO

Keywords:
Solid oxide fuel cells
Sealant
Torsion test
Finite element analysis
Shear strength

ABSTRACT

A torsion test recently implemented for solid oxide fuel cell sealant materials is analyzed as a method for measuring the shear strength of sealant for solid oxide fuel cells. The finite element method is used to simulate the stress distribution in the hourglass-shaped steel specimens with intermediate sealant layer with different specimen's dimensions and configurations. Also, it is analyzed how stress concentration changes if the sealant does not completely fill the gap or is squeezed out of gap. The reduction of seal thickness to outer radius ratio results in an increase in stress concentration at the outer edge of sealant. The developed specimens with a hollow halve steel plate as well as the ones with two hollow halve steel plates appear to be suitable choices for torsional shear strength test, reducing the torque for fracture and stress concentrations. Effects of lack of filling and squeezing out of gap onto the stress distribution are negligible compared to the effect of pre-existing discontinuities.

1. Introduction

Solid oxide fuel cells (SOFCs) are promising devices for future clean energy production. The planar SOFC (pSOFC) with metallic interconnects can be categorized as an advanced generation SOFC following stacks based on tubular cells and planar cells with ceramic interconnects [1]. In principle, pSOFCs are ceramic composite sheets of anode, electrolyte and cathode layer. The cells are fixed and sealed in metallic housings and interconnected by metallic plates to form a stack [2]. Glass-ceramic sealants are considered as among the most promising materials for a gas tight sealing of pSOFCs [3].

The presence of dissimilar materials and also temperature gradients in the stack lead to generation of strains during steady state operation as well as heating and cooling. As a consequence tensile as well as shear stresses are generated that can lead to failure [4,5]. In order to model the mechanical behavior of a stack, designers need the pure tensile and pure shear strengths of the joined components, in particular of the sealants. Although a number of studies have been carried out concentrating on bending [6–8] and tensile [9–12] tests to evaluate the pure tensile fracture stress of sealants, only a limited number of studies exist on shear strength evaluation [13–15].

In fact, it has been verified that the torsion test on hourglass-shaped specimens is an appropriate shear testing technique for ceramic joints by the virtue of its pure shear loading, relatively low stress concentration, and easy alignment [16]. The first efforts to characterize SOFC sealants by this method were made on miniature specimens [17,18]. The group at Jülich has developed more recently a shear test based on the same approach for larger specimens in order to obtain properties representative for the geometry in a real SOFC stack [19]. The shear stress distribution (τ) in a section subjected to torsion can be calculated straight forward with Eqs. (1) and (2):

$$\tau = \frac{T}{J}x \tag{1}$$

$$J = \frac{\pi}{2}(R_o^4 - R_i^4) \tag{2}$$

where T is the torque, J the sectional polar moment of inertia, x the radial coordinate, R_o and R_i are outer and inner radiuses. The nominal shear strengths are calculated by substituting fracture torque and R_o for T and x in Eq. (1).

The torsion tests on a glass-ceramics reinforced with either YSZ fibers or Ag particles (Fig. 1) have indicated that the size of specimens can affect the results [18,19]. It can be seen that overall, the large specimens lead to lower shear strengths compared to miniature ones. The arrows in Fig. 1 represents large specimens that have not broken at the torque limit of set-up (220 N m). Based on weakest link theory, the

* Corresponding authors at: Department of Materials Science and Engineering, Sharif University of Technology, Azadi Avenue, P. O. Box 11155-9466, Tehran, Iran.
E-mail addresses: fakouri@mehr.sharif.ir (M. Fakouri Hasanabadi), faghihi@sharif.edu (M.A. Faghihi-Sani), kokabi@sharif.edu (A.H. Kokabi), j.malzbender@fz-juelich.de (J. Malzbender).

http://dx.doi.org/10.1016/j.ceramint.2017.06.128
Received 2 June 2017; Received in revised form 19 June 2017; Accepted 20 June 2017
Available online 21 June 2017

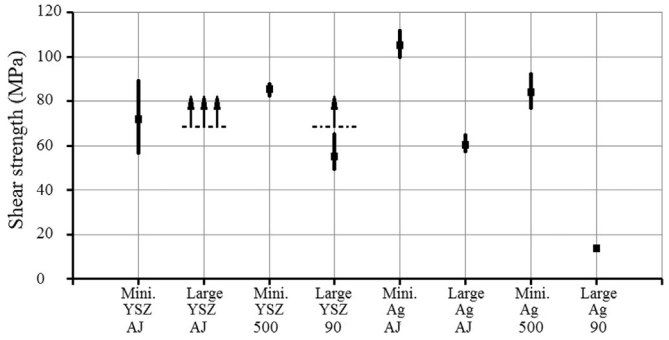

Fig. 1. The shear strength low-high-close chart of the composite sealants obtained with miniature and large hourglass-shaped specimens [18,19]. AJ: as joined, 500: annealed at 800 °C for 500 h, 90: annealed at 850 °C for 90 h.

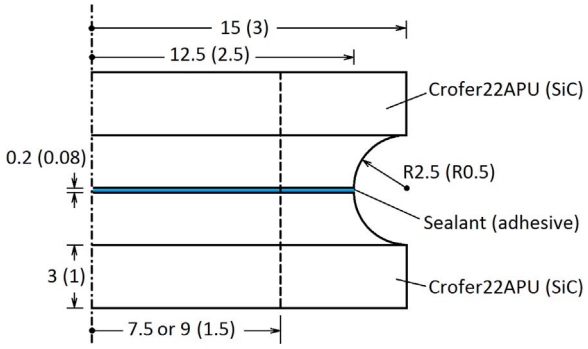

Fig. 2. Schematic of large hourglass-shaped specimens. The characteristics in parentheses are representative for the miniature specimens [21]. The dimensions are in mm.

Table 1
Properties of the materials used in the analysis.

Material	Young's modulus E (GPa)	Poisson's ratio ν (-)	Ref.
SiC	466	0.21	[21]
Glass-ceramics adhesive	140	0.25	[21]
Glass-ceramics sealant	75	0.25	[23]
Crofer22APU	200	0.3	[23]

larger specimens have a higher probability of containing a larger defect, which in turn can cause lower strengths [20]. Such behavior which is more probable for brittle materials can be described by analyzing the measured data on the basis of Weibull statistics. But, first of all, it

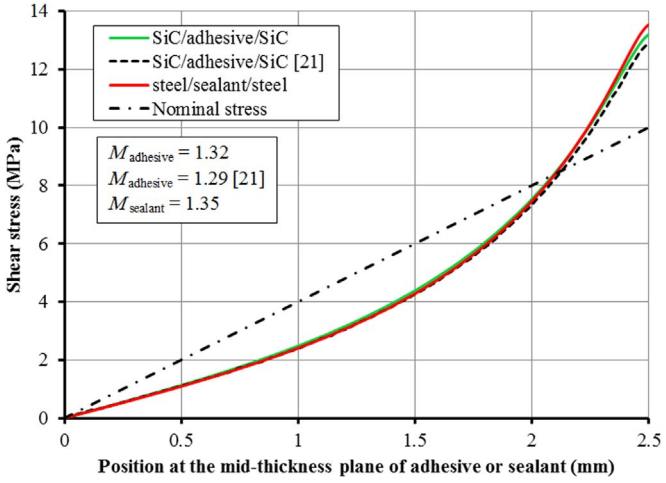

Fig. 4. FE results for miniature full-full specimens.

should be determined how close the measured/calculated stresses are to true values. Recently, a finite element modeling of the test for miniature specimens [21] has shown that a non-negligible stress concentration arises, which must be taken into account to assess the strength in terms of true stress (especially for comparison of different geometries).

In the current paper, the stress distribution for large specimens with different configurations is investigated. Also, it is analyzed how stress concentration is changed if the sealant does not completely fill the gap (LOF) or is squeezed out of gap (SqO), geometrical variations that are typical for the real joining situation [22]. For this purpose, numerical simulations using finite element analyses (FEA) have been performed.

2. Finite element analyses (FEA)

A three-dimensional (3D) model was developed using finite element software (ANSYS Workbench 18) to simulate the shear stress distribution in specimens. The initial simulation results revealed that due to the square geometry a maximum 4% difference in stresses at the outer edge of sealant arises compared to simplified cylinder geometry. As the mesh had to be extremely refined near the interface, it was deemed that the deviation from axial symmetry in the square ends of the specimen did not affect its central portion. Therefore, the mesh size was optimized (reduced to 2.5×10^{-3} mm at the edges of sealant) for an axisymmetric model. To warrant the model as well as mesh size

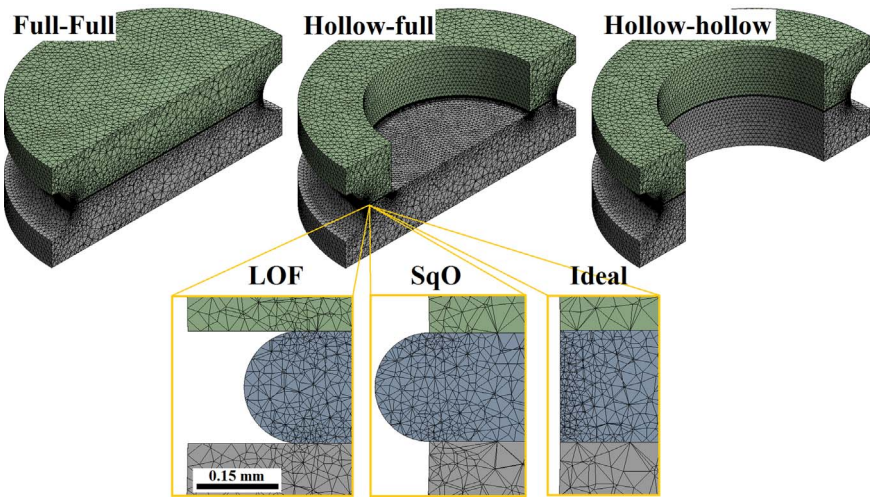

Fig. 3. 3D finite element models for different configurations of hourglass-shaped specimens.

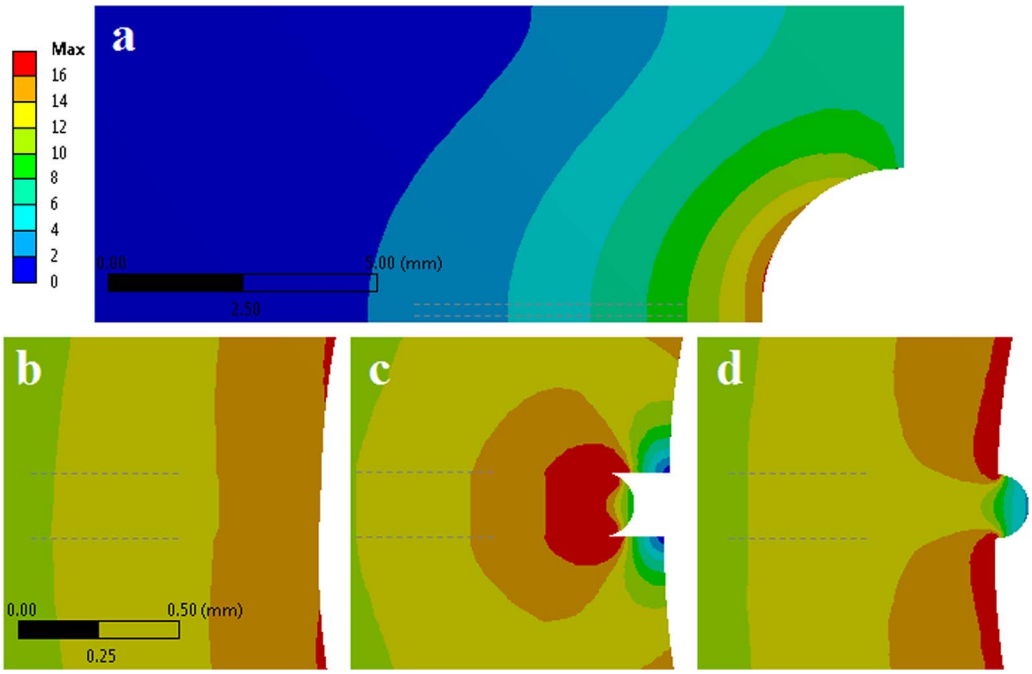

Fig. 5. Contour plot of the shear stress (MPa) in the large full-full specimens under torsion: a) overall view and details near the edge for b) ideal, d) LOF and c) SqO conditions.

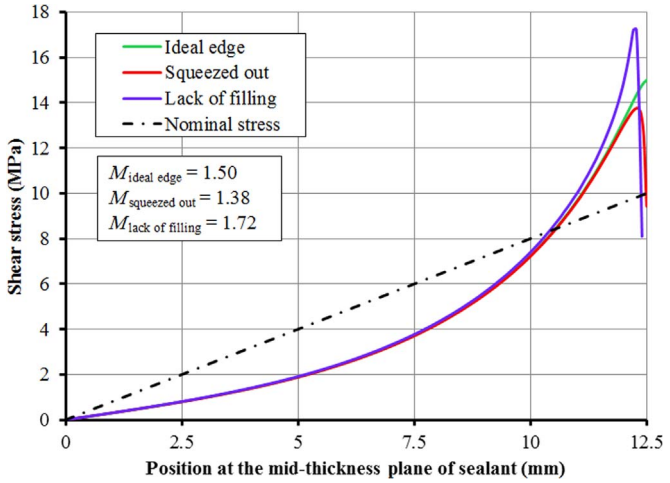

Fig. 6. FE results for large full-full specimen and the effect of SqO and LOF conditions.

optimization, some 3D finite element simulations were also carried out on the specimen geometry considered by Goglio and Ferraris (miniature specimens, Fig. 2) and compared with their 2D simulation results [21]. Fig. 2 shows a schematic of the rather large hourglass-shaped specimens, also presenting for comparison the dimensions of miniature ones. Table 1 shows the elastic properties considered for the materials. Both joining materials (sealant and adhesive) are kinds of glass-ceramic which, considering their application and joined material, have different properties.

The main affecting parameter in comparison of miniature and large specimens is the seal thickness to outer radius ratio which is 32×10^{-3} (0.08/2.5) and 16×10^{-3} (0.2/12.5), respectively. Fig. 3 shows the three configurations which were investigated; full-full (with full halves), hollow-full (consisting both hollow and full halves) and hollow-hollow (with hollow halves). All large hollow halves have an inner radius of 9 mm, except for a large hollow-hollow specimen which has 7.5 mm holes and is specified here by 7.5hollow-hollow. To obtain a result that is more representative for reality, a curvature with a radius of 0.1 mm was assumed for edges of sealants. Also, it was considered in additional complementary simulation what happens if the sealant does not fill about 0.2 mm (LOF) of the gap or is squeezed about 0.1 mm out (SqO) of gap at the edges.

3. Results and discussion

Similarly to that reported by Goglio and Ferraris [21], the tensile and compressive stress evaluations showed that the stress states in the cross-section of all specimens are of pure shear. Fig. 4 shows the shear stress distribution in the mid-thickness plane of glass-ceramics (adhesive in [21] or sealant in the current study) for miniature specimens. The torque values which were used as input in the models/calculations were defined to create a peak nominal shear stress in the glass-ceramic of 10 MPa (values calculated by means of Eq. (1) with x equal to 2.5 mm). The stress concentration factor (M) determines the ratio of peak actual to peak nominal shear stresses. As can be seen in Fig. 4, the results for SiC/adhesive/SiC joint are almost the same as that reported by Goglio and Ferraris [21], and M values (1.32 and 1.29) are close to each other.

Fig. 5 shows the contour plot of the shear stress in the larger full-full specimens. Similar results were obtained for the hollow-hollow specimen, which are however not shown for brevity. The evaluation of the shear stresses at the mid-thickness plane of sealant (Figs. 4 and 6) illustrated higher M of these specimens relative to miniature ones ($1.50 > 1.35$), which would also be higher (1.75) if there is LOF condition. As it can be seen in Fig. 5b–d, the stress distribution near the outer edge of specimen strongly depends on how the sealant fills the gap. Both, the SqO and LOF conditions result in a high stress concentration at the triple-phase boundaries steel/sealant/atmosphere.

Fig. 7 shows the contour plot of the shear stress in hollow-full specimens. There is a localized stress concentration at the inner edge of the sealant, in the vicinity of full half (Fig. 7b), which however, in reality might be affected by local SqO and LOF conditions. The shear stress plot at the mid-thickness plan of sealant for hollow-full specimens (Fig. 8a) illustrates that shear stress at the inner edge does not exceed that at the outer edge. These specimens show smaller stress concentration than full-full ones ($M = 1.23 < 1.50$, Figs. 6 and 8a).

Fig. 8a shows that the M values for miniature hollow-hollow and

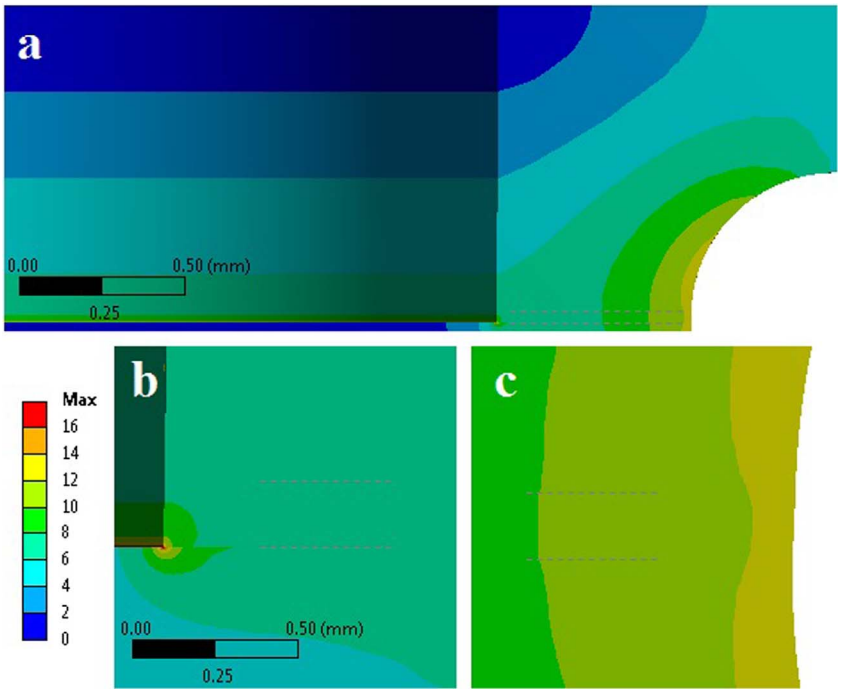

Fig. 7. Contour plot of the shear stress (MPa) in the large hollow-full specimen under torsion: a) overall view, and details on b) inner and c) outer edges.

large 7.5hollow-hollow specimens are 1.26 and 1.37, respectively. The ratio of thickness to other dimensions of sealant in miniature hollow-hollow specimens is twice that in large 7.5hollow-hollow ones. Therefore, reduction of this ratio to half results in 11% and 9% increase in stress concentration at respectively full-full and hollow-hollow specimens (Figs. 6 and 8a). However, it can be also seen in Fig. 8a that increase of inner radius (from 7.5 mm to 9 mm) has compensated for seal thickness reduction, and M values for both miniature and large hollow-hollow specimens are 1.26. Therefore, the hollow-hollow and hollow-full specimens, in addition to reduction of stress concentration, can eliminate the effect of specimen's size. Also, annulus-shape sealants in hollow-hollow and hollow-full specimens appear to tolerate an about 37% lower torque than the disk-shape sealant in full-full specimens. Therefore, the hollow-hollow and hollow-full configurations might be a good choice in cases where the load limitation of set-up is a problem.

Fig. 8b indicates that the LOF condition is more effective in increasing the stress concentration in hollow-hollow specimens (16%) than in full-full specimens (13%), this is related to the fact that the LOF is considered in both inner and outer edges, and thus the area for load bearing has been decreased more. Considering the high stress concentration (M) at the triple-phase boundaries steel/sealant/atmosphere of some specimens (Fig. 5c and d), as well as higher possibility of failure at these points [3], the stress distribution at the edge of sealant seems to be important. Fig. 9 shows the stress distribution at the edges of sealants. The LOF and SqO conditions cause a high stress concentration at the triple-phase boundaries steel/sealant/atmosphere, which might lead to micro-crack initiation and gradual propagation. The pre-existing discontinuities (pores) in the sealant exceed in size 20 μm [18] which, in addition to stress concentration, might deflect or blunt micro-cracks. Therefore the effects of LOF and SqO relative to pre-existing discontinuities appear not to be significant.

For hollow-full specimens, the shear stress exceeds 12.3 MPa (the stress at the outer edge) at a limited area (1 μm) near the full half at the inner edge (Figs. 7b and 9). Although this area reaches the critical shear stress at a lower applied torque than the outer edge, it appears to be too small to create a crack longer than critical size for fracture and hence to initiate cracking in comparison with the outer edge. Therefore the resulting cracks appear to grow gradually starting from the inner edge during the constant strain rate loading. During the test, eventually the shear stress at the outer edge exceeds the critical value and macroscopic cracking will occur. The stress gradient at the outer edge (Fig. 8a) is low and hence the resulted cracks can quickly grow and lead to fracture.

Compared to full-full specimens, hollow-full and hollow-hollow specimens should show higher nominal shear stresses in the torsional test due to lower M at the edge of their sealants. However, it has been recently reported that both miniature hollow-hollow and full-full specimens yielded the same nominal shear stress [17]. However, the FEM results confirm the presence of localized stresses at particular regions. Future work on subcritical crack growth might permit to gain more insight into the effect of localized stresses on fracture behavior.

4. Conclusions

In this study, the finite element method was used to investigate the effect of hourglass-shaped specimen's dimensions and configuration on shear stress distribution during the torsional test. The main conclusions of this study are summarized below.

- The ratio of thickness to outer radius of sealant has a significant effect on shear stress distribution at the sealant. The reduction of this ratio, which takes place for large specimens, results in an increase in stress concentration at the outer edge of sealant. Of course the reduction of this ratio can be compensated by increasing the inner radius of sealant.
- The specimen with two hollow halves (or one hollow half) and annulus-shape sealant can decrease the required torque for fracture, and also has the lower stress concentration. Therefore, they are the attractive alternative configurations to the specimen with full halves and disk-shaped sealant.
- A shear stresses concentration can take place at the triple-phase boundaries steel/sealant/atmosphere if the sealant does not completely fill the gap or is squeezed out of gap. But their effects are negligible relative to of pre-existing discontinuities.

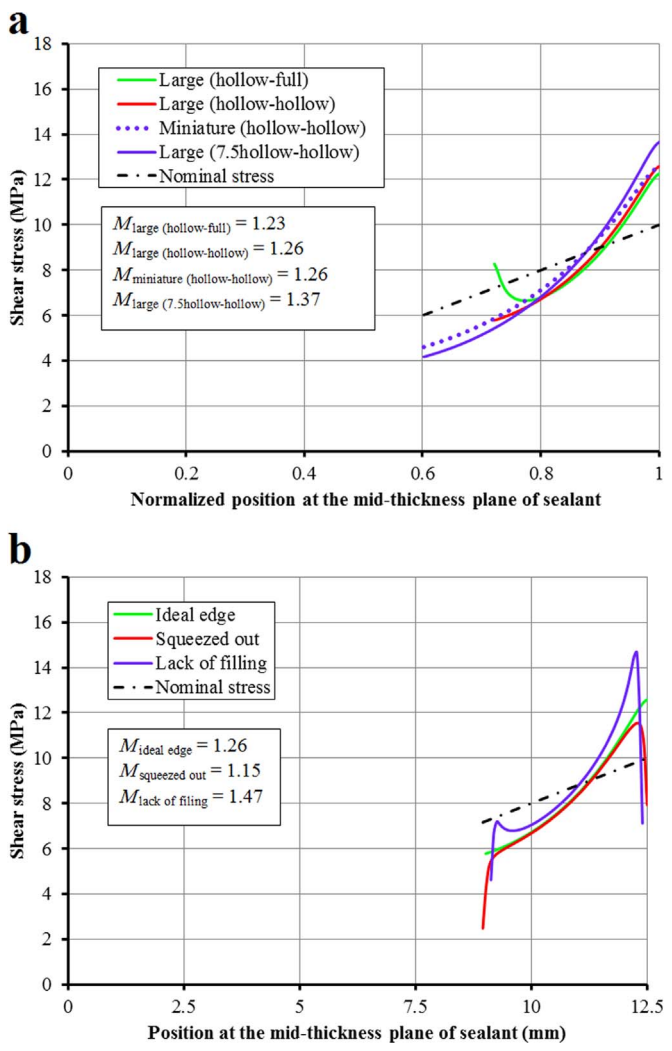

Fig. 8. FE results for a) hollow-full and hollow-hollow specimens at normalized positions (divided by R_o), b) large hollow-hollow specimens considering ideal edge as well as SqO and LOF conditions.

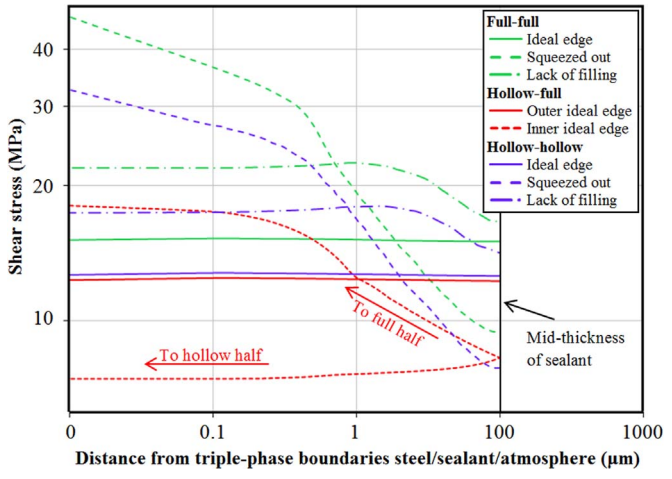

Fig. 9. FE results along the thickness of the glass. Due to asymmetrical distribution at the inner edge of the hollow-full specimen, its curves have been shown in both directions.

Acknowledgements

The authors wish to thank Ms. T. Osipova for the support in specimens testing, Dr. S.M. Groß-Barsnick and Mr. D. Federmann for supportive discussions on sealant materials aspects, and also Prof. L. Singheiser and Prof. M. Krüger for hosting at Forschungszentrum Jülich. We also express our gratitude to research board at Sharif University of Technology.

References

[1] H. Yokokawa, N. Sakai, History of high temperature fuel cell development, in: W. Vielstich, H.A. Gasteiger, A. Lamm, H. Yokokawa (Eds.), Handb. Fuel Cells, John Wiley & Sons, Ltd, Chichester, UK, 2010. http://dx.doi.org/10.1002/9780470974001.f104012.

[2] B. Kuhn, F.J. Wetzel, J. Malzbender, R.W. Steinbrech, L. Singheiser, Mechanical performance of reactive-air-brazed (RAB) ceramic/metal joints for solid oxide fuel cells at ambient temperature, J. Power Sources 193 (2009) 199–202. http://dx.doi.org/10.1016/j.jpowsour.2008.10.117.

[3] M. Fakouri Hasanabadi, A.H. Kokabi, A. Nemati, S. Zinatlou Ajabshir, Interactions near the triple-phase boundaries metal/glass/air in planar solid oxide fuel cells, Int. J. Hydrog. Energy 42 (2017) 5306–5314. http://dx.doi.org/10.1016/j.ijhydene.2017.01.065.

[4] L. Blum, S.M. Groß, J. Malzbender, U. Pabst, M. Peksen, R. Peters, et al., Investigation of solid oxide fuel cell sealing behavior under stack relevant conditions at Forschungszentrum Jülich, J. Power Sources 196 (2011) 7175–7181. http://dx.doi.org/10.1016/j.jpowsour.2010.09.041.

[5] J. Malzbender, Curvature and stresses for bi-layer functional ceramic materials, J. Eur. Ceram. Soc. 30 (2010) 3407–3413. http://dx.doi.org/10.1016/j.jeurceram-soc.2010.07.036.

[6] Y. Zhao, J. Malzbender, Elevated temperature effects on the mechanical properties of solid oxide fuel cell sealing materials, J. Power Sources 239 (2013) 500–504. http://dx.doi.org/10.1016/j.jpowsour.2013.04.043.

[7] J. Malzbender, Y. Zhao, T. Beck, Fracture and creep of glass–ceramic solid oxide fuel cell sealant materials, J. Power Sources 246 (2014) 574–580. http://dx.doi.org/10.1016/j.jpowsour.2013.08.010.

[8] J. Wei, G. Pećanac, J. Malzbender, Mechanical behavior of silver reinforced glass–ceramic sealants for solid oxide fuel cells, Ceram. Int. 41 (2015) 15122–15127. http://dx.doi.org/10.1016/j.ceramint.2015.08.084.

[9] F. Smeacetto, M. Salvo, M. Ferraris, V. Casalegno, P. Asinari, A. Chrysanthou, Characterization and performance of glass–ceramic sealant to join metallic interconnects to YSZ and anode-supported-electrolyte in planar SOFCs, J. Eur. Ceram. Soc. 28 (2008) 2521–2527. http://dx.doi.org/10.1016/j.jeurceram-soc.2008.03.035.

[10] S.-M. Gross-Barsnick, C. Babelot, D. Federmann, U. Pabst, Optimization of tensile strength measurements on glass-ceramic sealant used for SOFC stacks, ECS Trans. 68 (2015) 2573–2582. http://dx.doi.org/10.1149/06801.2573ecst.

[11] C.-K. Lin, Y.-A. Liu, S.-H. Wu, C.-K. Liu, R.-Y. Lee, Joint strength of a solid oxide fuel cell glass–ceramic sealant with metallic interconnect in a reducing environment, J. Power Sources 280 (2015) 272–288. http://dx.doi.org/10.1016/j.jpowsour.2015.01.126.

[12] M. Fakouri Hasanabadi, A. Nemati, A.H. Kokabi, Effect of intermediate nickel layer on seal strength and chemical compatibility of glass and ferritic stainless steel in oxidizing environment for solid oxide fuel cells, Int. J. Hydrog. Energy 40 (2015) 16434–16442. http://dx.doi.org/10.1016/j.ijhydene.2015.10.023.

[13] J. Malzbender, J. Mönch, R.W. Steinbrech, T. Koppitz, S.M. Gross, J. Remmel, Symmetric shear test of glass-ceramic sealants at SOFC operation temperature, J. Mater. Sci. 42 (2007) 6297–6301. http://dx.doi.org/10.1007/s10853-006-1178-1.

[14] E.V. Stephens, J.S. Vetrano, B.J. Koeppel, Y. Chou, X. Sun, M.A. Khaleel, Experimental characterization of glass – ceramic seal properties and their constitutive implementation in solid oxide fuel cell stack models, J. Power Sources 193 (2009) 625–631. http://dx.doi.org/10.1016/j.jpowsour.2009.02.080.

[15] A. Selçuk, A. Atkinson, Measurement of mechanical strength of glass-to-metal joints, Fuel Cells 15 (2015) 595–603. http://dx.doi.org/10.1002/fuce.201500028.

[16] C. Shih, Y. Katoh, J.O. Kiggans, T. Koyanagi, H.E. Khalifa, C.A. Back, et al., Comparison of Shear Strength of Ceramic Joints Determined by Various Test Methods with Small Specimens, 2015, pp. 139–149. doi: ⟨http://dx.doi.org/10.1002/9781119040323.ch13⟩. (in:).

[17] F. Smeacetto, A. De Miranda, A. Ventrella, M. Salvo, M. Ferraris, Shear strength tests of glass ceramic sealant for solid oxide fuel cells applications, Adv. Appl. Ceram. 114 (2015) S70–S75. http://dx.doi.org/10.1179/1743676115Y.0000000042.

[18] B.C. Greven, Glass-Ceramic Sealant Reinforcement for High-Temperature Applications, RWTH Aachen, Aachen, Germany, 2015 ⟨http://juser.fz-juelich.de/record/200841⟩.

[19] T. Osipova, J. Wei, G. Pećanac, J. Malzbender, Room and elevated temperature shear strength of sealants for solid oxide fuel cells, Ceram. Int. 42 (2016) 12932–12936. http://dx.doi.org/10.1016/j.ceramint.2016.05.064.

[20] M.W. Barsoum, Fundamentals of Ceramics, IOP Publishing Ltd, Bristol, 2003.

[21] L. Goglio, M. Ferraris, Bonding of ceramics: an analysis of the torsion hourglass specimen, Int. J. Adhes. Adhes. 70 (2016) 46–52. http://dx.doi.org/10.1016/j.ijadhadh.2016.05.006.

[22] P. Batfalsky, J. Malzbender, N.H. Menzler, Post-operational characterization of solid oxide fuel cell stacks, Int. J. Hydrog. Energy 41 (2016) 11399–11411. http://dx.doi.org/10.1016/j.ijhydene.2016.05.065.

[23] J. Malzbender, T. Wakui, R.W. Steinbrech, Curvature of planar solid oxide fuel cells during sealing and cooling of stacks, Fuel Cells 6 (2006) 123–129. http://dx.doi.org/10.1002/fuce.200500109.